

First-principles free energies and Ginzburg-Landau theory of domains and ferroelectric phase transitions in BaTiO₃

Anil Kumar and Umesh V. Waghmare

Theoretical Sciences Unit, Jawaharlal Nehru Centre For Advanced Scientific Research, Jakkur, Bangalore 560064, India

(Received 23 May 2010; published 25 August 2010)

We present a method based on combination of (a) constrained polarization molecular dynamics and (b) thermodynamic integration to determine the free-energy landscape relevant to structural phase transitions and related phenomena in ferroelectric materials, bridging the gap between first-principles calculations and phenomenological Landau-type theories. We illustrate it using a first-principles effective Hamiltonian of BaTiO₃ to (a) uncover the quantitative features of the free-energy function that are responsible for its first-order ferroelectric transitions, (b) calculate the minimum free-energy pathways for the polarization switching and (c) evaluate temperature-dependent free energy of domain walls, and a minimum free-energy pathway to formation of ferroelectric domains. We use our method within a variational mean-field theory to connect with Landau theory and show through comparison with numerically exact simulations that (a) the state constrained to have vanishing order (away from the equilibrium) below the transition temperature is highly degenerate due to fluctuations that drive the phase transition first order, and (b) certain terms need to be added to the phenomenological Landau-Devonshire free-energy functions to capture the physics of spatial fluctuation in order parameter. Our method can be readily generalized to any classical microscopic Hamiltonian and ensembles characterized with a given constraint.

DOI: [10.1103/PhysRevB.82.054117](https://doi.org/10.1103/PhysRevB.82.054117)

PACS number(s): 77.80.Fm, 77.80.bg, 77.80.Dj

I. INTRODUCTION

Ferroelectric materials are important to technologies based on microelectromechanical systems, random access memories, capacitors, transducers, and other applications.^{1,2} While first-principles simulations³ have played a significant role in developing a fundamental understanding of properties and phase transitions in these materials, phenomenological Landau-type theories^{4–6} are very useful in understanding phenomena at long length and times scales, and particularly in simulations of devices.^{7,8} It is highly desirable to establish a rigorous link between these two descriptions, which would (a) provide a precise picture of the nature of these phase transitions and (b) allow multiscale simulations of ferroelectric structures.

BaTiO₃, a simple example of ferroelectric perovskites,^{9,10} undergoes a succession of three phase transitions from high-temperature cubic structure to tetragonal (C \leftrightarrow T), tetragonal to orthorhombic (T \leftrightarrow O), and orthorhombic to rhombohedral (O \leftrightarrow R) ferroelectric phases with decrease in temperature. The direction of the spontaneous polarization in these ferroelectric phases is typically along a crystallographic axis. For example, tetragonal, orthorhombic, and rhombohedral ferroelectric phases are characterized by polarization along [001], [011], and [111] directions, respectively.

It is known from experiments as well as first-principles calculations that the ferroelectric phase transitions in BaTiO₃ involve small atomic displacements and strain deformations of the high-temperature equilibrium cubic structure.^{11,12} Experimentally measured and local-density-approximation-calculated phonon dispersions show that only lowest-energy transverse-optical (TO) modes (soft modes) and long-wavelength acoustic modes make significant contributions to properties of low-temperature phases. Based on these observations, Zhong *et al.* used an approximation that the energy

surface relevant to ferroelectric transition could be expressed as a function of acoustic, soft TO mode amplitudes and strain, reducing the number of degree of freedom (DoF) per unit cell from 15 to 6. Expressing this energy surface formally as a Taylor expansion in these DoFs, they obtained a simple effective Hamiltonian, which can be readily simulated using molecular dynamics (MD) or Monte Carlo methods to study phenomena with longer time and length scales. This approximation for an effective Hamiltonian works well for high- T_c ferroelectrics, and a more complete microscopic Hamiltonian including order-disorder terms would be appropriate for materials with low T_c .

We note that the effective Hamiltonian captures the low-energy landscape of BaTiO₃ associated with degrees of freedom that include complete bands of soft optical phonons, acoustic phonons, and six components of homogeneous strain. Acoustic phonons describe the local or inhomogeneous strain, whose coupling with polarization leads to long-range elastic interactions, which often have important consequences to domain walls in ferroelectrics.

Earlier, there has been an attempt to link the first-principles-based Monte Carlo simulations to the Landau-Devonshire phenomenological theory by Iniguez *et al.*¹³ They used polarization histograms obtained in Monte Carlo simulations to estimate free energies associated with ferroelectric transitions in BaTiO₃. In their study, the quadratic coefficient in Landau-Devonshire free-energy function, which determines the free energy close to zero polarization state, was obtained by interpolating the exact free-energy data at temperatures away from the transition. In such an approach, detailed access to microstates relevant to the transition is not readily possible. Recently, Geneste¹⁴ used a Lagrange's multiplier technique to constrain polarization and thermodynamics integration (TI) to determine changes in free energies. Our method presented here is similar in spirit

but based on Legendre transform of the Hamiltonian to constrain polarization. We also demonstrate its use in a variational mean-field theory to obtain Landau free energies as well as generalization to obtain free energies of inhomogeneously ordered (polarized) states of ferroelectrics, such as ones with domains.

Using our method, based on a combination of constrained polarization MD and TI, in the FERAM (Refs. 15 and 16) implementation of molecular dynamics of first-principles ferroelectric model Hamiltonian of BaTiO₃,^{11,12} we calculate free-energy differences between a state with arbitrary configuration of polarization and the one with zero polarization. We aim to answer the following questions: (a) what is the free-energy landscape as a function of polarization? (b) What is the nature of the ferroelectric phase transitions and which DoFs are crucial to it? (c) What is the free-energy barrier for polarization switching? and (d) how does the domain-wall energy vary as a function of temperature and what is the minimum free-energy path and barrier between the uniformly polarized configuration and a configuration with domains?

We show that the Landau-Devonshire free energy of states with polarization close to the zero for $T < T_c$ is accessible using *only* mean-field theory, where spatial fluctuations are suppressed. In this case, the quadratic coefficient of Landau-Devonshire free-energy expansion decreases linearly with temperature changing its sign at T_c^{MFT} . However, our “exact” simulations of ferroelectric ($T < T_c$) phases constrained to vanishing polarization reveal a high degeneracy associated with states with spatial fluctuations with vanishing energy cost, which drive the phase transition to a first-order type. Such a degeneracy can result in unusual properties of the free-energy function, as was pointed in the context of one-dimensional model of structural transition.⁶

In Sec. II, we present the formalism and tests of our methodology. We present results of our exact and mean-field analysis of ferroelectric transitions in Sec. III. Our analysis of BaTiO₃ with domains is presented in Sec. IV and our results for estimation of free-energy barriers for polarization switching are presented in Sec. V. We finally summarize our work in Sec. VI.

II. COMPUTATIONAL METHODS

A. MD with constrained homogeneous polarization

For constraining polarization at a given value in molecular-dynamics simulations, we augment the effective Hamiltonian H_0 of BaTiO₃, obtained from the first-principles calculations^{11,12,17} through addition of three terms (like in Legendre transformation),

$$H = H_0 - Z^* \vec{E} \cdot \sum_i \vec{\xi}_i + \Omega \vec{P} \cdot \vec{E} - \frac{\Omega}{8\pi} \sum_{\alpha\beta} (\epsilon_{\alpha\beta}^\infty - \delta_{\alpha\beta}) E_\alpha E_\beta \quad (1)$$

where $\vec{\xi}_i$ is the polar Wannier-type¹⁸ vector (i being the lattice site) mapping to displacements of atoms clustered at site i , Z^* is the Born effective charge associated with the polar

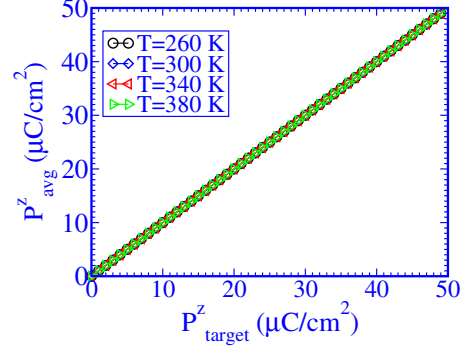


FIG. 1. (Color online) Average polarization vs target polarization at different temperatures in constraint polarization molecular-dynamics simulations.

soft mode, \vec{E} is an auxiliary fluctuating electric field, \vec{P} is the target polarization, and Ω is the total volume of the system. Born effective charges are determined using Berry phase approach. Since our simulations are classical MD simulations, they do not need explicit implementation of Berry phase approach but are consistent with its results at the first-principles level. Maximization of H (dielectric response $\epsilon_{\alpha\beta}^\infty = \epsilon^\infty$ for the cubic symmetry) with respect to E gives

$$\vec{E} = \frac{4\pi}{(\epsilon^\infty - 1)} \left(\vec{P} - \frac{Z^* \sum_i \vec{\xi}_i}{\Omega} \right), \quad (2)$$

where \vec{E} is an effective auxiliary electric field that maintains the total polarization of the system at a *constraint* value \vec{P} . Substituting variational value of electric field [Eq. (2)] in Eq. (1),

$$H = H_0 + \frac{1}{2} \frac{4\pi\Omega}{(\epsilon^\infty - 1)} \left(\vec{P} - \frac{Z^* \sum_i \vec{\xi}_i}{\Omega} \right)^2. \quad (3)$$

The second term in Eq. (3) is a harmonic confining potential that forces polarization distribution in an MD simulation to be centered at the constrained value of polarization. As a result, use of the modified Hamiltonian H [given by Eq. (3)] ensures sampling in molecular-dynamics simulations to yield target average polarization obtained in the simulations (see Fig. 1).

The partition function of a system with Hamiltonian H [Eq. (3)] is given by

$$Z_H(\vec{P}) = \int \prod_i d\vec{\xi}_i \exp \left(- \frac{H_0 + \frac{2\pi\Omega}{(\epsilon^\infty - 1)} \left(\vec{P} - \frac{Z^* \sum_i \vec{\xi}_i}{\Omega} \right)^2}{k_B T} \right) \quad (4)$$

and corresponding free energy of the system is

$$F_H(\vec{P}) = -k_B T \ln Z_P + \frac{3}{2} k_B T \ln \left[\frac{(\epsilon^\infty - 1) k_B T}{2\Omega} \right], \quad (5)$$

where Z_P is the partition function of system at constrained polarization in the *absence of external electric field*¹⁹ and we

have used the Gaussian approximation of Dirac delta function for the constraint on polarization,

$$Z_{\vec{P}} = \int \prod_i d\vec{\xi}_i \delta\left(\vec{P} - \frac{Z^* \sum_i \vec{\xi}_i}{\Omega}\right) \exp\left(-\frac{H_0}{k_B T}\right). \quad (6)$$

The second term in Eq. (5), which is proportional to $\frac{1}{\Omega}$, vanishes as $\Omega \rightarrow \infty$. The derivative of free energy with respect to polarization is the average auxiliary field,

$$\frac{\partial F_H}{\partial \vec{P}} = \Omega \left\langle \frac{4\pi}{(\epsilon^\infty - 1)} \left(\vec{P} - \frac{Z^* \sum_i \vec{\xi}_i}{\Omega} \right) \right\rangle_H, \quad (7)$$

where $\langle \rangle_H$ represent ensemble average with Hamiltonian H .

We use thermodynamic integration method²⁰ to calculate free-energy differences of the system between the states characterized by values of order parameter P_2 and P_1 ,

$$\Delta F_H = \int_{\vec{P}_1}^{\vec{P}_2} \langle \vec{E}(\vec{P}') \rangle d\vec{P}'. \quad (8)$$

B. MD with constraint on states with inhomogeneous polarization

We now generalize our method to study the configurations characterized by a constraint on thermodynamic average of an arbitrary microstate (a configuration of degrees of freedom) of the system, e.g., a domain wall. This is accomplished through a general form of Hamiltonian,

$$H = H_0 - \mathbf{E}^D \cdot Z^* \sum_i \hat{e}_i \cdot \xi_i + \Omega \mathbf{P}^D \cdot \mathbf{E}^D - \frac{\Omega(\epsilon^\infty - 1)}{8\pi} \mathbf{E}^{D2}, \quad (9)$$

where superscript D means domain (or it can be a configuration characterized by spatially dependent polarization) and \hat{e}_i is the unit vector along the direction of this configuration in the phase space. For a configuration with domains, if we set $\hat{e}_i = \hat{z}$ for site i belong to a region of the first domain in the system and $\hat{e}_i = -\hat{z}$ for site i belong in the second domain separated by a domain wall. This leads to the formation of two 180° domain walls separating the two domains in periodic boundary conditions.

Generalized domain polarization is obtained through maximization with respect to E^D ,

$$\mathbf{P}^D = \frac{(\epsilon^\infty - 1)}{4\pi} \mathbf{E}^D + \frac{Z^* \sum_i \hat{e}_i \cdot \xi_i}{\Omega}, \quad (10)$$

which is zero for uniformly polarized state.

C. Mean-field theory

To be able to connect with Landau theory, we also study properties of H in the mean-field approximation where spatial fluctuations are suppressed. The general form of first-principles effective Hamiltonian of BaTiO₃ is

$$H = \sum_i H_0(\xi_i) + \sum_{ij} \mathbf{J}_{ij} \xi_i \xi_j, \quad (11)$$

where i is the index of a site and \mathbf{J}_{ij} includes all the interactions in the system. (We note that we treat thermal fluctuations in strain exactly in our analysis, and it amounts to integrating them out analytically.) In the mean-field theory, we map this interacting many-body Hamiltonian into a single-particle effective Hamiltonian using a self-consistent mean field f as

$$\tilde{H} = \sum_i H_i = \sum_i H_0(\xi_i) + \mathbf{f} \sum_i \xi_i. \quad (12)$$

Free energy of the system of this noninteracting Hamiltonian is

$$F(f, p) = -k_B T \ln \int \prod_i d\xi_i \exp\left[-\frac{p\left(\frac{\mathbf{J}^0 \mathbf{p}}{N} - f\right) + \tilde{H}}{k_B T}\right], \quad (13)$$

where $\mathbf{J}^0 = \sum_{ij} \mathbf{J}_{ij}$. The self-consistency condition on polarization $\langle \sum_i \xi_i \rangle_{\tilde{H}} = p$ is obtained through a variational principle for $F(f, p)$ with respect to f , giving the mean-field Landau theory. For practical calculations, we determine free-energy differences, in the mean-field approximation, of a configuration with polarization P and with respect to that with a zero polarization using thermodynamic integration,

$$\Delta F = \frac{2\mathbf{J}^0}{N} \int_0^P \left\langle \sum_i \xi_i \right\rangle dp - \frac{\mathbf{J}^0 P^2}{N}. \quad (14)$$

We implemented the above exact and mean-field formalisms in the mixed-space molecular-dynamics code “FERAM”^{15,16,21} in which infinite long-range interactions are treated in the reciprocal space.^{22,23} We use Nose-Poincare thermostat²⁴ for the constant temperature which allow us to use relatively large time step of 2 fs. Our simulations are carried out for systems of size $L_x \times L_y \times L_z$ with periodic boundary conditions. For a given temperature, we start the simulation from a equilibrated zero polarization initial configuration and increase the polarization in the step of 1 $\mu\text{C}/\text{cm}^2$. For each value of polarization, we thermalize the system with 100 000 time steps, and do thermal averaging is using configurations of subsequent 100 000 time steps. We find these time steps are sufficient for equilibration of the system in the temperature range studied and we have tested the convergence of free energy with respect to number of time steps. Second, we have also tested our methodology through calculation of the free-energy differences between two configurations by carrying out thermodynamic integration along different paths connecting them and making sure that they are path independent.

III. ANALYSIS OF FERROELECTRIC TRANSITIONS IN BaTiO₃

A. Free energies of ferroelectric transitions in BaTiO₃

First, we report our results for the free-energy landscape of ferroelectric transitions as a function of polarization and

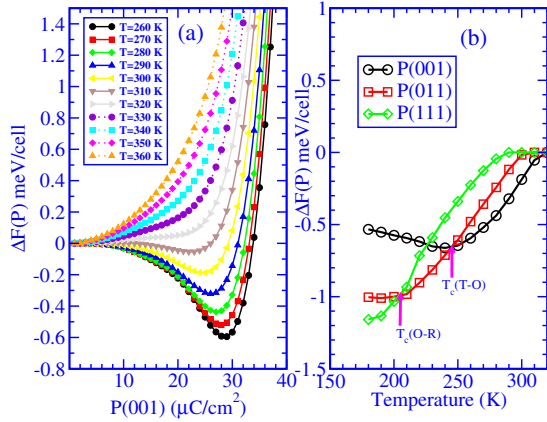


FIG. 2. (Color online) (a) Free-energy differences per unit cell with respect to vanishing polarization ($P=0$) as a function of polarization along [001] direction for different temperatures, and (b) minimum of the free-energy difference per unit cell as a function of temperature along [001], [011], and [111] directions of polarization.

temperature. We determine free energy as a function of polarization in the [001], [011], and [111] directions with zero polarization as the reference state at each temperature. At high temperatures ($T > 326$ K), the free energy has a single well form with one minimum at vanishing polarization. As temperature is decreased below 316 K, free energy of a state with P along [001] direction becomes lower for nonzero values of polarization compared to that with vanishing polarization and system undergoes a transition from the cubic perovskite to tetragonal (C \rightarrow T) structure. With further decrease in temperature free energies corresponding to nonzero value of polarization along the [011] and [111] directions become lower compared to that with vanishing polarization at temperatures of 300 K and 290 K, respectively (see Fig. 2). However, at these temperatures the free energies of states with P along [011] and [111] directions are higher in free energy than the tetragonal (P along [001] direction) one. Below $T=245$ K, free energy of the state with P along [011] direction becomes lowest among the three and system undergoes a transition from tetragonal to orthorhombic structure. Subsequently, free energy of the rhombohedral state with P along the [111] direction becomes the lowest among the three at $T=205$ K and the system undergoes a transition from an orthorhombic to a rhombohedral structure. Our estimated values of spontaneous polarization for tetragonal, orthorhombic, and rhombohedral phases are 28, 34, and 43 $\mu\text{C}/\text{cm}^2$ which are the same as earlier calculations¹¹ and are close to the experimental values given by Mitsui *et al.*²⁵

To develop more confidence in our methodology and confirm the temperatures of tetragonal-orthorhombic and orthorhombic-rhombohedral transitions through determination of free energies along two independent polarization paths, for example, we determined the free-energy differences as a function of polarization along paths (a) [000 \rightarrow 001], [001 \rightarrow 011], and [011 \rightarrow 111], and (b) [000 \rightarrow 011] and [000 \rightarrow 111]. These simulations show ferroelectric transitions at 245 K along the path [001 \rightarrow 011], and at 205 K along the path [011 \rightarrow 111]. The changes in free energy for path with P along [000 \rightarrow 111] and that with combined paths

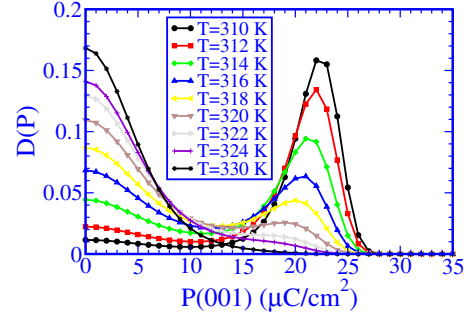


FIG. 3. (Color online) Polarization probability distribution function as defined in text near the cubic to tetragonal transition temperature.

of P along [000 \rightarrow 011] and [011 \rightarrow 111] are the same. Similarly, the free energy of the orthorhombic phase obtained along a path with P along [000 \rightarrow 011] and along a combined path of P along [000 \rightarrow 001] and [001 \rightarrow 011] are the same. Thus, our free-energy-based estimates of transition temperatures match those obtained earlier through direct Monte Carlo¹¹ and MD simulations²¹ validating our methodology, and corresponding free energies are path independent demonstrating internal consistency.

B. Nature of the C-T phase transition in BaTiO₃

To probe the first-order character of the C-T transition in BaTiO₃, we examine the polarization probability distribution function $D(\mathbf{P})$ (defined as $\propto \exp(-\beta\Delta F(P))$) close to the transition temperature. It exhibits seven peaks (six corresponding to symmetry equivalent states with polarization along [001] direction and one at vanishing polarization) of equal height at $T=316$ K (see Fig. 3), confirming the first-order nature of the C-T phase transition. Seven peaks are visible over a narrow temperature range from 304 to 322 K, corresponding to local minima in the free-energy function. This is expected to be the range of temperature for coexistence of C and T phases. The presence of seven peaks is in contrast to first-order transitions (such as liquid-solid transition) characterized by a third-order term in Landau free-energy function. In the present case, the cubic symmetry of the high-symmetry phase does not allow the third-order term, and the first-order character of such transitions is expected from the fourth-order term in free energy being negative (as shown in the next section). Six of the seven peaks in polarization distribution or minima in the free-energy function correspond to different orientation of the ordered phase, and suggest that spatial fluctuations in order parameter (different orientations of P in different spatial regions = domains, with $\nabla \cdot \vec{P} = 0$ as we will show later) cost vanishingly small energy in the thermodynamic limit, the energy cost coming from the domain walls. We note that the magnitude of the free-energy barrier separating various local minima [for e.g., $\pm P(001)$] is very small, and is expected to be related to domain-wall energies.¹⁹ Our free-energy-based analysis provides a physical picture of the fact that C-T transition in BaTiO₃ is a fluctuation driven first-order transition.^{26–28}

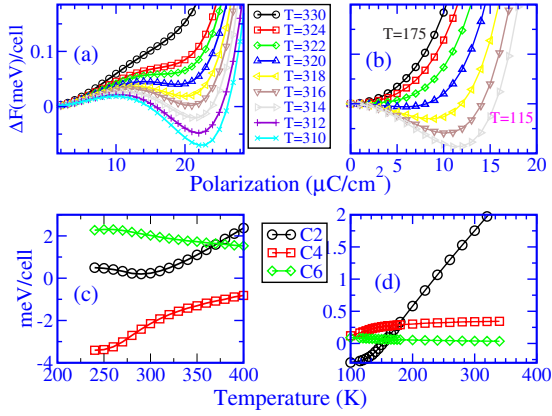


FIG. 4. (Color online) Free-energy landscape near the cubic to tetragonal transition temperature when (a) strain-polarization coupling is present, and (b) strain coupling is turned off. The second-, fourth- and sixth-order free-energy expansion coefficients as a function of temperature when (c) strain-polarization coupling is present, and (d) strain-polarization coupling is turned off.

To quantify the features of free-energy function relevant to the first-order C-T transition, we determine the temperature dependence of Landau free-energy expansion coefficients by fitting calculated free energies to a sixth-order polynomial in polarization given as $\Delta F(P) = C_2 P^2 + C_4 P^4 + C_6 P^6$, where C_2, C_4, C_6 are second-, fourth-, and sixth-order coefficients, respectively (we find that higher-order polynomials do not give better fit). The fourth-order coefficient in Landau free-energy functional [see Fig. 4(c)], is negative at all temperature close to the ferroelectric transition temperature and responsible for the first-order phase transition. The second-order coefficient, which is proportional to the phonon frequency, decreases linearly with decrease in temperature close to $T = T_c$ corresponding to the well-known softening of the polar TO phonon near ferroelectric transition. However, it anomalously increases below T_c [see Fig. 4(c)], which seems to suggest that “cubic paraelectric?” phase is locally stable even below T_c . This is indeed puzzling in light of the standard picture based on Landau theory, and we now discuss its microscopic origin.

We determine the nature of the phase with vanishing polarization below T_c through examination of a snapshot of a microstate sampled during an MD simulation with total polarization constrained to zero. It is clear (see Fig. 5) that such a constraint leads to stabilization of states with spatial fluctuations

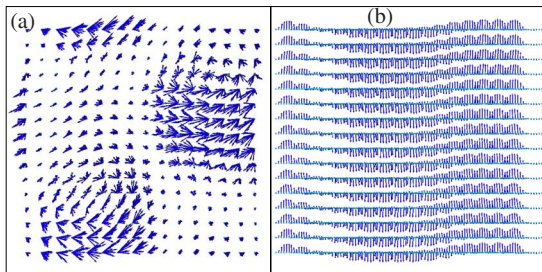


FIG. 5. (Color online) The snapshots of formation of oscillatory spatial fluctuations of polarization for the constrained vanishing polarization ($P=0$) at $T=280$ K, (a) top view and (b) side view.

in polarization. Thus, $P=0$ state for $T < T_c$ is *not* a cubic paraelectric but indeed a ferroelectric one consisting of domains. We emphasize that this finding about the reference $P=0$ state in exact statistical mechanics analysis below T_c is in contrast to the one in Landau theory, and exact free energies thus determined should be interpreted with care. The energy barrier (well depth), for $T \leq T_c$, in exactly calculated free-energy landscape actually relates to the energies of domain walls. Our analysis provides a simple understanding why the parameter C_2 remains positive and that it does not reflect the stability of paraelectric phase below T_c . We note that a state with similar fluctuating order parameter is also stable for nonvanishing values of constrained polarization (smaller than its equilibrium value) below T_c .

As is known from the earlier work on ferroelectric phase transitions,²⁹ the third-order coupling between strain ($e_{\alpha\beta}$) and polarization ($H \sim g e_{\alpha\beta} P_\gamma$) is crucial to the first-order character of the C-T phase transition. We now determine the free-energy landscape when this coupling is switched off. In this case, the free-energy landscape as a function of polarization and temperature, does not exhibit any free-energy barrier between states with zero and nonzero values of polarization for $T \geq T_c$ [see Fig. 4(b)]. Indeed, the second order coefficient C_2 varies linearly as a function of temperature and becomes negative below $T=155$ K [see Fig. 4(d)], and the fourth- and the sixth-order coefficients remain positive at all temperatures. We thus confirm from the free-energy picture that it is the strain-polarization coupling which leads to the first-order transition in BaTiO₃. We note that the transition temperature is also significantly reduced with respect to that obtained with effective Hamiltonian with a strain-polarization coupling. This is largely due to the fact that effect of negative pressure^{11,12} is nullified when the strain coupling is switched off. To meaningfully compare the T_c 's with and without strain-polarization coupling, we estimated *exact* transition temperature with zero pressure, which is $T_c = 175$ K. Thus, the reduction in T_c due to neglect of strain-polarization coupling is only about 20 K.

C. Mean-field theory

To access Landau-Devonshire free-energy landscape, in which the reference state with vanishing polarization is a paraelectric phase, we now present our analysis by suppressing spatial fluctuations in order parameter (which were shown to be unavoidable in exact analysis above) within a mean-field approximation [as described in Sec. II C]. Determining free energies as a function of polarization along [001], [110], and [111] directions, we find that transition occurs from cubic to rhombohedral phase at $T=900 \pm 20$ K. In the mean-field theory, the relative stability of T, O, and R phases is determined by the fourth-order term in free-energy expansion. We find that R phase is always lower in energy than T and O, though errors in our estimates of the free-energy differences for temperatures close to T_c are a bit large (see Fig. 6). In contrast to the exact analysis, the second-order coefficient in Landau free-energy expansion as a function of temperature varies linearly near T_c and vanishes at T_c . It is negative below the transition temperature while the

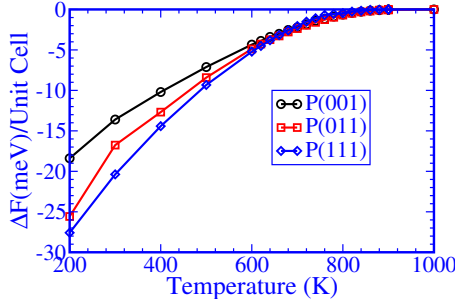


FIG. 6. (Color online) Mean-field results: free energy per cell with respect to vanishing polarization ($P=0$) as a function of temperature along different directions of polarization.

fourth-order coefficient is always positive. This picture is very much the as one expected within Landau theory of second-order phase transitions. We note that this analysis includes the strain-polarization coupling in the effective Hamiltonian. We also carried out mean-field analysis of the effective Hamiltonian switching off the strain-polarization coupling. The nature of phase transition here remains the same as above, with a transition temperature of about 500 K. Large reduction in T_c here is also mostly from the effect of negative pressure¹¹

Thus, we clearly establish that (a) strain-polarization coupling and (b) spatial fluctuations in order parameter are essential to the physics of first-order ferroelectric phase transitions. At low temperatures far from T_c , polarization is expected to saturate,³⁰ and a more generalized form of Landau free-energy functional is desirable.

While the temperature dependence of second-order coefficient of our Landau free-energy functional is similar to those in other flavors of Landau theory, it and other coefficients are not expected to be comparable to phenomenological theories because ours is a Landau-type theory derived from first principles. Thus, it compares well with similar works of Iniguez¹³ and Geneste.¹⁴ However, it is different from the phenomenological theory, as our transition temperatures are very different from the experimental ones to which a phenomenological Landau theory is fit to (Ref. 31).

D. Free energy of spatial fluctuations in the order parameter

While the mean-field theory gives an expected behavior of C_2 (as in Landau theory) below the transition temperature, it (a) yields a wrong order of phase transitions and (b) overestimates the transition temperatures greatly. The mean-field theory is not quite adequate to capture the physics of ferroelectric transitions in BaTiO₃. As the spatial fluctuations in the order parameter have been shown here to be responsible for this, we now propose a way of developing a phenomenological theory that goes beyond the standard Landau-type theory: we consider addition of terms to the Landau free-energy function to include effects of spatial fluctuations in order parameter,

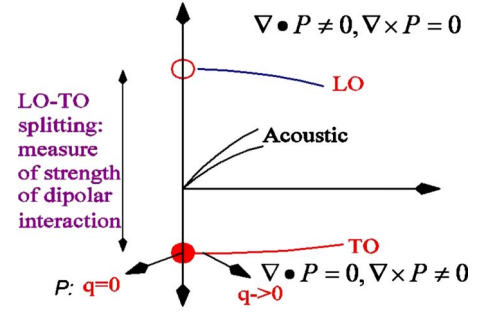


FIG. 7. (Color online) Schematic showing that the presence of spatial inhomogeneity of polarization in the ferroelectrics leads to LO-TO splitting of phonon modes at Γ point.

$$\begin{aligned}
 F(\vec{P}, T) = & F(0, T) + C_2(T) \int d\vec{r} |\vec{P}(r)|^2 + C_{41}(T) \int d\vec{r} P_x^4(r) \\
 & + P_y^4(r) + P_z^4(r) + C_{42}(T) \int d\vec{r} |\vec{P}(r)|^4 + C_{41}^s(T) \\
 & \times \left[\sum_{\alpha} \int d\vec{r} P_{\alpha}^2(r) \right]^2 + C_{42}^s(T) \\
 & \times \left[\sum_{\alpha \neq \beta} \int d\vec{r} P_{\alpha}(r) P_{\beta}(r) \right]^2 + C_6(T) \int d\vec{r} |\vec{P}(r)|^6 \\
 & + C_8(T) \int d\vec{r} |\vec{P}(r)|^8 + U \int d\vec{r} |\nabla \cdot \vec{P}(r)|^2 \\
 & + V \int d\vec{r} |\nabla \times \vec{P}(r)|^2 \\
 & + \frac{1}{2\epsilon^{\infty}} \int d\vec{r} d\vec{r}' \frac{[\nabla \cdot \vec{P}(r)][\nabla' \cdot \vec{P}(r')]}{|r - r'|} \quad (15)
 \end{aligned}$$

Low-energy spatial fluctuations in the polarization field are expected to vary with a long wavelength, i.e., optical phonons in the $q \rightarrow 0$ limit (see Fig. 7). Polarization modes with nonzero curl and vanishing divergence are the TO modes, and the ones with nonzero divergence and vanishing curl are the longitudinal optical modes. Thus the term depending on $\nabla \times \vec{P}$ captures the dispersion of branch of polar TO modes near $q=0$ and the first term depending on $\nabla \cdot \vec{P}$ captures the dispersion of branch of LO modes. The last term depending on divergence of P contains the long-range dipole-dipole interactions, and reproduces the LO-TO splitting at Γ point in a ferroelectric. The quartic terms with coefficients C_{41}^s and C_{42}^s arise from the coupling of polarization with strain. If the strain is integrated out (using a Gaussian integral) from the partition function, it is straightforward²⁹ to show the emergence of this term. Clearly, it has a negative coefficient and connects with the negative quartic coefficient of free-energy function in the exact analysis. It is evident from this free-energy functional of the polarization field that the $P=0$ states with minimum free energy at $T < T_c$ will be inhomogeneous, consisting of spatial fluctuations in P typical of a combination of modes in the polar TO branch.

We note that the physics of strain and its coupling with polarization are considered in our analysis, as it was done in

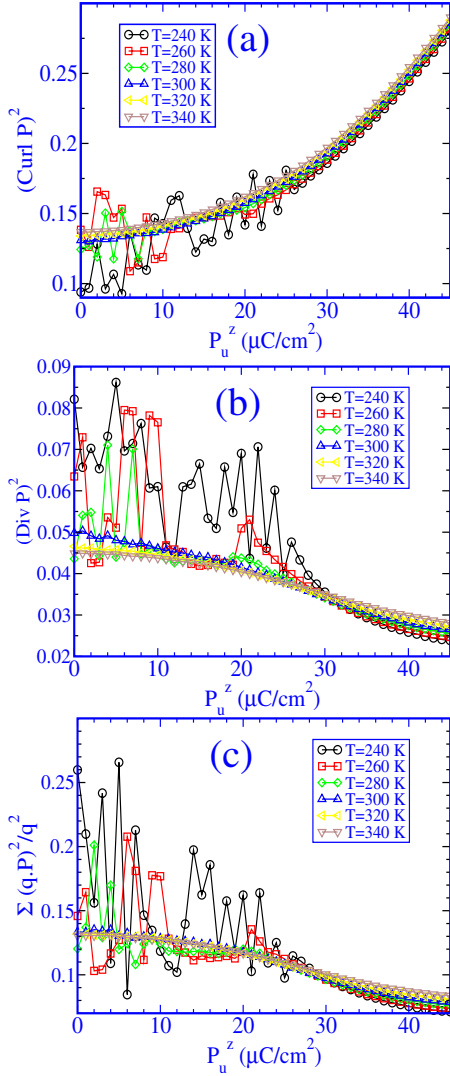


FIG. 8. (Color online) Thermodynamically averaged spatial fluctuations in the constrained polarization simulations (a) $\int d\vec{r} |\nabla \times \vec{P}|^2$, (b) $\int d\vec{r} |\nabla \cdot \vec{P}|^2$, and (c) $\int d\vec{r} d\vec{r}' \frac{|\nabla \cdot \vec{P}(r) \nabla \cdot \vec{P}(r')|}{r-r'}$.

the Ref. 11. The present analysis of free-energy functional depends explicitly on only polarization, as the strain has been integrated out.

Fitting of exactly calculated free energies to this modified free-energy functional [Eq. (15)] is rather tricky, as the states with $P=0$ at $T < T_c$ are highly degenerate! A clear evidence for this is obtained by examining thermodynamics averages of $\int d\vec{r} |\nabla \times \vec{P}|^2$, $\int d\vec{r} |\nabla \cdot \vec{P}|^2$, and $\int d\vec{r} d\vec{r}' \frac{|\nabla \cdot \vec{P}(r) \nabla \cdot \vec{P}(r')|}{r-r'}$ as functions of polarization and temperature (see Fig. 8). Indeed, these quantities are quite noisy for polarization below a “critical” value of polarization when $T < T_c$. A careful examination of different snapshots of configurations from MD reveals any translational symmetry operation (for example, translation of domain walls in Fig. 5) or rotation gives rise to newer configurations with the same free energy. Since the dispersion of the low-energy TO branch (Fig. 7) is rather weak, it is clear that the energies of states with these modes frozen are infinitesimally close to energy of ferroelectric state. Inclusion of these terms leads to better fit to calculated free energies.

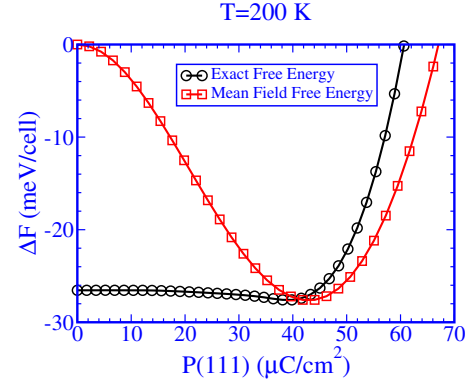


FIG. 9. (Color online) A comparison of free energies obtained from the exact analysis and the mean-field calculation as a function of polarization at $T=200$ K.

Comparison of free-energy landscapes obtained with exact analysis and within mean-field theory is also subtle due to large difference in the estimates of transition temperatures in the two schemes. Nevertheless, we compare the free-energy landscape at low temperature ($T=200$ K) and find a drastic difference in the magnitude of the free-energy barrier (see Fig. 9). In light of the microscopic picture developed so far, this is not surprising. While the free-energy barrier in exact analysis related to domain-wall energies and vanishes¹⁹ in the thermodynamic limit: $[\Delta F = (2L^2 \gamma_D + E_{FE} L^3)]/L^3$, where γ_D is the domain-wall energy per unit area, E_{FE} is the free-energy gain due to uniform polarization, and L is size of the system], the barrier estimated within mean-field theory converges ($T \rightarrow 0$) to the barrier associated with double well form of the total energy surface obtained within first-principles density-functional theory (DFT).

IV. FREE ENERGY AND NUCLEATION OF DOMAINS

Using the generalized Hamiltonian [Eq. (9)], which can be used to study systems consisting of domains or any inhomogeneous configurations of polarization, we obtained free energy as a function of domain polarization [P_D as defined in Eq. (10)] at different temperatures [see Fig. 10(a)]. We start with a uniformly polarized state (for which the domain polarization $P_D=0$) and increase P_D in step of $1 \mu\text{C}/\text{cm}^2$. At a given temperature, uniform polarization changes discontinuously [see Fig. 10(b)] at a certain value of P_D . With further increase in P_D , the free energy is essentially constant (nearly flat part of the free-energy curve) up to P_D =the spontaneous polarization at that temperature, and increases subsequently. To understand this path to formation of ferroelectric domains, we determined planar-averaged polarization [perpendicular to the x axis and defined as $P(x) = \sum_{(y,z)} P(x,y,z)$]. Evolution to the state with ferroelectric domains starts with nucleation of a small domain with opposite polarization in one half of the system. The discontinuous change in uniform polarization at a higher value of P_D is associated with formation of a wide (≈ 2 nm) domain wall in the system [see Fig. 10(c)]. Finally, the flat region of the free-energy curve is associated with narrowing of the width of the domain wall,

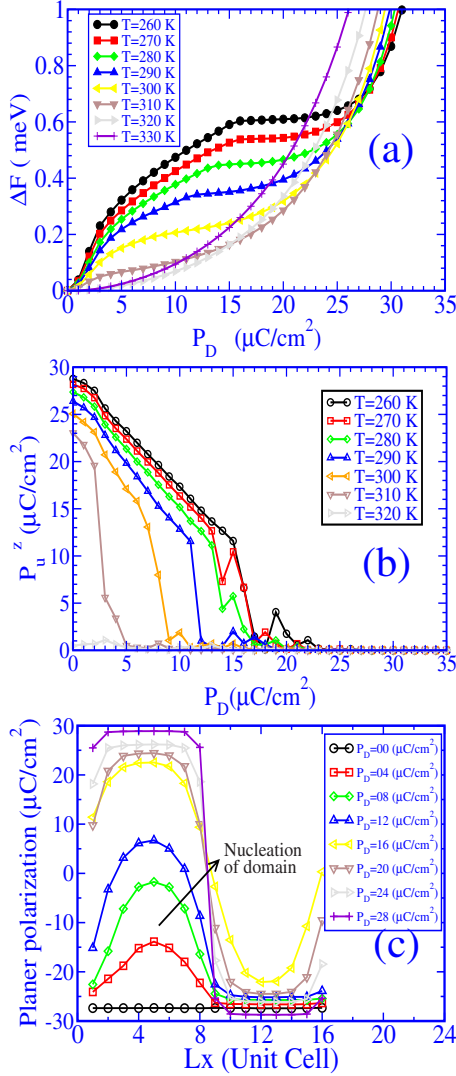


FIG. 10. (Color online) (a) Free-energy landscape as a function of domain polarization, (b) evolution of uniform polarization from a uniform polarized state to a state with one up and one down domains as a function of P_D in a system of size $16 \times 16 \times 16$ unit cell, and (c) planer-averaged polarization perpendicular to L_x for different values of domain polarization at $T=280$ K.

which becomes atomically sharp (width=1 unit cell) at $P_D = P_s(T)$.

Nucleation in ferroelectric is a nonperturbative phenomenon, which is reflected in a highly nonlinear free-energy function that we determine [see Fig. 10(a)] as a function of nucleation coordinate (P_D). As system evolve from a uniformly polarized state (say, a stable state) to a state consist of up and down domains (say, a metastable state with a domain-wall analogous to a soliton), we find a nucleus of domain with opposite polarization is formed as seen in Fig. 10(c), accompanied by a sharp increase in free energy at values of $P_D \leq 14 \mu\text{C}/\text{cm}^2$ [see Fig. 10(a)]. Once a nucleus of large enough size is formed, system discontinuously jumps to a state with up and down polarization in two domains separated by a thick domain wall. Upon further evolution, the domain wall sharpens without much energy cost [the flat region of free energy in Fig. 10(a)] and becomes thin on the

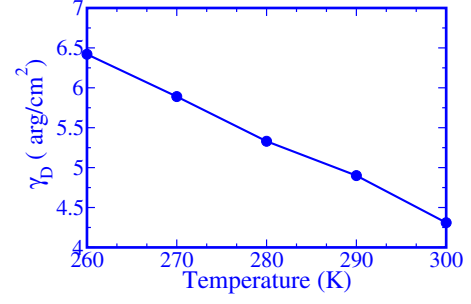


FIG. 11. (Color online) Domain-wall free energy as a function of temperature.

atomic cell (a few unit cells). This domain wall in the final configuration is indeed analogous to a soliton.³² In fact the free energy determined here can be used in the phenomenological soliton-based theory of domain dynamics.³²

The domain-wall energy at a temperature is obtained from $\gamma_D(T) = \Delta F(P_D = P_s) / (2L_y L_z)$, where P_s is the spontaneous polarization of the system at that temperature. The factor of 2 is due to two domain walls present in our systems under periodic boundary conditions. Our estimate of the domain-wall energy as a function of temperature (see Fig. 11) and domain-wall thickness are comparable to that estimated with a $T=0$ K calculation based on DFT (Ref. 33) and reported in the experimental work of Merz.³⁴

The domain-wall energy can be shown from the free-energy function [Eq. (15)] to be proportional to VP_s^2/a^2 , where a is the lattice constant, and V relates to the dispersion of TO phonons near $q=0$: $w^2(q) = w_0^2(1 + Vq^2)$. Thus, the temperature dependence of the domain-wall energy arises from that of spontaneous polarization and that of dispersion of the branch containing the soft TO mode.

We note that other inhomogeneous configurations of polarization, for example, twin walls,³⁵ can also be analyzed with our technique while treating effects of homogeneous and inhomogeneous (acoustic modes) strain coupling in effective Hamiltonian exactly. However, effects of coupling of polarization to other optical phonon modes are not included in the effective Hamiltonian itself, and they could be relevant to more accurate analysis of twin walls.³⁵

V. POLARIZATION SWITCHING: DOMAINS VERSUS P ROTATION

Polarization switching with electric field (PE-hysteresis) is a very important property of a ferroelectric that (a) characterizes a material to be a ferroelectric, and (b) make is useful for computer memory applications. We now use the knowledge of free energies to understand the mechanisms of polarization switching, restricting ourselves to bulk ferroelectrics, which by definition is *homogeneous*, without considering effects of its interface with electrodes or extrinsic inhomogeneities. We assess the role of two competing mechanisms of polarization switching: (a) one by polarization evolution along a minimum free-energy path that connects the state with polarization P to that with polarization $-P$, and (b) the one that is forced to go through nucleation

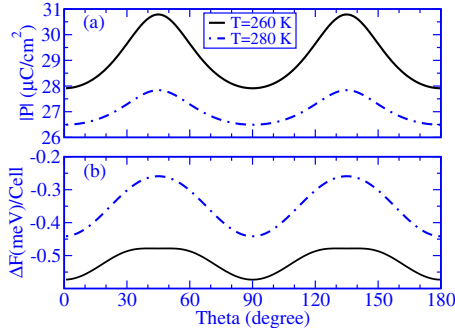


FIG. 12. (Color online) (a) The magnitude of polarization along minimum free-energy path as a function of rotation angle (minimum energy path is one in which polarization rotates through the orthorhombic phase, see text), and (b) free-energy barrier for the polarization switching from P along $[001]$ to P along $[00\bar{1}]$ direction.

and growth of a domain with opposite polarization.

Using the constrained polarization method, we estimated free-energy barrier and a minimum free-energy pathways for polarization switching in BaTiO_3 . For example, the system is stable along $[001]$ direction of polarization at $T=280\text{ K}$. We estimate the free-energy barrier for polarization switching by evolving it along a path defined from $[001]$ to $[00\bar{1}]$. We constrain only the P_z component along line connecting these two minima and allow the other two components (P_x and P_y) to relax to the minimum free energy. From our results for P_x , P_y and P_z , we find that P rotates in the zx or zy plane [see Fig. 12(a)], consistent with earlier reports.^{36–38} Our estimate for this barrier at $T=260\text{ K}$ is lower (0.1 meV/cell) than that at $T=280\text{ K}$ (0.18 meV/cell) [see Fig. 12(b)]. The state along the switching path corresponding to the maximum (barrier) is the orthorhombic phase, and hence it is understandable why the barrier is lower at $T=260\text{ K}$: as the system undergoes a transition to orthorhombic phase at $T=245\text{ K}$ and its free energy relative to tetragonal phase decreases with temperature. We confirmed these results also through determination of the minimum free-energy pathway and barrier using the functional form of the free-energy landscape determined earlier.

From our results for free-energy barrier for P rotation (which scales with volume of the system and given as $\Delta F^R = f^R \cdot L_x \cdot A$, where f^R is the energy barrier for polarization rotation per unit cell and A is domain-wall area) and free energy of a domain wall (which scales with cross-sectional area of the system and barrier is given as $\Delta F^D = 2\gamma_D \cdot A$), we conclude that polarization switching through formation of domains would be favored only if the width of the system is larger than a critical size ($L_x^c = \frac{2\gamma_D}{f^R}$). When the width of sys-

tem is smaller than this critical size, ferroelectric BaTiO_3 would switch its polarization through rotation. This finding should have implications to use of ferroelectrics to miniaturized memory devices.

VI. SUMMARY

We have presented a method based on a combination of constrained polarization MD and thermodynamic integration to determine free-energy landscape of ferroelectric materials starting from first-principles effective Hamiltonian. We demonstrated this methodology through application to BaTiO_3 , obtaining (a) a clear picture of fluctuation-driven first-order phase transitions that it exhibits, and (b) free energetics relevant to mechanisms of its polarization switching. Our method of constrained polarization is very general and applicable to any Hamiltonian, it can be readily used to study the domain dynamics in bulk as well as in the finite systems, and we plan to use in the study of kinetics of nucleation and growth of polarization domains in ferroelectric materials. Our approach can also be used to predict thickness dependence of coercive field and polarization switching time in thin films and understand their semiempirical behavior (laws) proposed by Merz.³⁹

Through a detailed microstates-based comparison between Landau mean-field and exact numerical analysis, we showed that the spatial fluctuations in polarization involving polar TO phonons (i.e., with $\nabla \times \vec{P} \neq 0$, $\nabla \cdot \vec{P} = 0$) are crucial to first-order character of the cubic to tetragonal phase transition, through their coupling with strain (the secondary order parameter). Based on this, we proposed a generalized phenomenological free-energy functional that depends on curl and div of polarization to capture the physics of fluctuations. The minimum free-energy pathways and barriers relevant to polarization switching determined here show that polarization switching in ferroelectrics should occur through formation of domains when the width of the system is larger than a temperature-dependent critical size, on the order of 6 to 20 nm.

ACKNOWLEDGMENTS

A.K. acknowledges Council of Scientific and Industrial Research (CSIR), India for research funding and Centre for Computational Material Science (CCMS), JNCASR for providing computational facilities. U.V.W. acknowledges funding from an IBM faculty and a DAE outstanding researcher grants. We thank stimulating discussions with T. V. Ramakrishnan, I. W. Chen, David Vanderbilt, and Karin M. Rabe.

¹J. F. Scott, *Science* **315**, 954 (2007).

²M. Dawber, P. Chandra, P. B. Littlewood, and J. F. Scott, *J. Phys.: Condens. Matter* **15**, L393 (2003).

³D. Vanderbilt, *Curr. Opin. Solid State Mater. Sci.* **2**, 701 (1997).

⁴D. Vanderbilt and M. H. Cohen, *Phys. Rev. B* **63**, 094108 (2001).

⁵A. J. Bell, *J. Appl. Phys.* **89**, 3907 (2001).

⁶A. P. Giddy, M. T. Dove, and V. Heine, *J. Phys.: Condens. Mat-*

- ter **1**, 8327 (1989).
- ⁷S. C. Hwang, J. E. Huber, R. M. McMeeking, and N. A. Fleck, *J. Appl. Phys.* **84**, 1530 (1998).
- ⁸E. B. Tadmor, U. V. Waghmare, G. S. Smith, and E. Kaxiras, *Acta Mater.* **50**, 2989 (2002).
- ⁹M. E. Lines and A. M. Glass, *Principles and Applications of Ferroelectrics and Related Materials* (Oxford University Press, New York, 1977).
- ¹⁰E. K. H. Salje, *Phase Transitions in Ferroelastic and Coelastic Crystals* (Cambridge University Press, Cambridge, 1990).
- ¹¹W. Zhong, D. Vanderbilt, and K. M. Rabe, *Phys. Rev. Lett.* **73**, 1861 (1994).
- ¹²W. Zhong, D. Vanderbilt, and K. M. Rabe, *Phys. Rev. B* **52**, 6301 (1995).
- ¹³J. Iniguez, S. Ivantchev, J. M. Perez-Mato, and A. Garcia, *Phys. Rev. B* **63**, 144103 (2001).
- ¹⁴G. Geneste, *Phys. Rev. B* **79**, 064101 (2009).
- ¹⁵<http://loto.sourceforge.net/feram>
- ¹⁶T. Nishimatsu, U. V. Waghmare, Y. Kawazoe, and D. Vanderbilt, *Phys. Rev. B* **78**, 104104 (2008).
- ¹⁷R. D. King-Smith and D. Vanderbilt, *Phys. Rev. B* **49**, 5828 (1994).
- ¹⁸K. M. Rabe and U. V. Waghmare, *Phys. Rev. B* **52**, 13236 (1995).
- ¹⁹K. Binder, *Rep. Prog. Phys.* **50**, 783 (1987).
- ²⁰D. Frenkel and B. Smith, *Understanding Molecular Simulations: From Applications to Algorithm* (Academic Press, New York, 2002).
- ²¹J. Paul, T. Nishimatsu, Y. Kawazoe, and U. V. Waghmare, *Phys. Rev. Lett.* **99**, 077601 (2007).
- ²²U. V. Waghmare, E. J. Cockayne, and B. P. Burton, *Ferroelectrics* **291**, 187 (2003).
- ²³B. P. Burton, E. Cockayne, and U. V. Waghmare, *Phys. Rev. B* **72**, 064113 (2005).
- ²⁴S. D. Bond, B. J. Leimkuhler, and B. B. Laird, *J. Comput. Phys.* **151**, 114 (1999).
- ²⁵T. Mitsui *et al.*, in *Ferroelectrics and Related Substances. Oxides*, edited by K.-H. Hellwege and O. Madelung, Landolt-Börnstein, New Series, Group III, Vol. 16 (Springer-Verlag, Berlin, 1981).
- ²⁶Y. Y. Goldschmidt, *Phys. Rev. B* **31**, 4369 (1985).
- ²⁷L. Radzihovsky and T. C. Lubensky, *Europhys. Lett.* **54**, 206 (2001).
- ²⁸S. A. Brazovskii, *Sov. Phys. JETP* **41**, 85 (1975).
- ²⁹K. M. Rabe and U. V. Waghmare, *Philos. Trans. R. Soc. London, Ser. A* **354**, 2897 (1996).
- ³⁰E. K. H. Salje, B. Wruck, and H. Thomas, *Z. Phys. B: Condens. Matter* **82**, 399 (1991).
- ³¹Y. L. Wang, A. K. Tagantsev, D. Damjanovic, N. Setter, V. K. Yarmarkin, A. I. Sokolov, and I. A. Lukyanchuk, *J. Appl. Phys.* **101**, 104115 (2007).
- ³²J. A. Krumhansl and J. R. Schrieffer, *Phys. Rev. B* **11**, 3535 (1975).
- ³³J. Padilla, W. Zhong, and D. Vanderbilt, *Phys. Rev. B* **53**, R5969 (1996).
- ³⁴W. J. Merz, *Phys. Rev.* **95**, 690 (1954).
- ³⁵L. Goncalves-Ferreira, S. A. T. Redfern, E. Artacho, and E. K. H. Salje, *Phys. Rev. Lett.* **101**, 097602 (2008).
- ³⁶H. Fu and R. E. Cohen, *Nature (London)* **403**, 281 (2000).
- ³⁷L. Bellaiche, A. Garcia, and D. Vanderbilt, *Phys. Rev. B* **64**, 060103 (2001).
- ³⁸J. Paul, T. Nishimatsu, Y. Kawazoe, and U. V. Waghmare, *Phys. Rev. B* **80**, 024107 (2009).
- ³⁹W. J. Merz, *J. Appl. Phys.* **27**, 938 (1956).